Article

Research on Braking Characteristics of Hybrid Excitation Rotary Eddy Current Retarder

Fei Wang [1], Wenguang Guo [1,*], Guijun Wu [2] and Shi Li [1]

1   School of Mechanical Engineering, Anyang Institute of Technology, Anyang 455000, China;
    wangfei@ayit.edu.cn (F.W.); h6636123zhuoyi@163.com (S.L.)
2   Department of Mechanics Engineering, Kyrgyz State Technical University Named after I. Razzakov,
    Aitmatov Av., 66, Bishkek 720044, Kyrgyzstan; wgj6666@126.com
*   Correspondence: 20200070@ayit.edu.cn

Abstract: According to the different excitation methods, automotive eddy current retarders (ECRs) can be divided into electrically excited retarders (EERs) and permanent magnet excited retarders (PMERs), and EERs and PMERs have certain complementarity in control and braking characteristics. Therefore, based on literature research, this article proposes a hybrid excitation rotary electromagnetic retarder (HERER) and conducts numerical simulation analysis and experimental research on the braking performance of the HERER. Firstly, the structure and working principle of the HERER are introduced. Secondly, based on the principles of electromagnetics, an equivalent magnetic circuit analysis model of the HERER is established. Then, a finite element analysis model of the HERER is established using Jmag 14 electromagnetic simulation software, and the braking performance of the HERER under different current and speed conditions is studied. Finally, bench tests are conducted on the air loss torque and eddy current braking performance of the HERER. The effectiveness of the finite element analysis model and equivalent magnetic circuit model of the HERER is verified.

1. Introduction

An eddy current retarder (ECR) is an auxiliary braking device that can effectively improve the safety of braking on long downhill slopes for large vehicles [1–3]. ECRs can be divided into electrically excited retarders (EERs) and permanent magnet excited retarders (PMERs) according to different excitation methods. The control method of an EER is simple and can quickly cut off the braking torque; however, due to its use of coil excitation, it inevitably has problems, such as heavy weight and high power consumption. Compared with EERs, PMERs have a higher braking power density and do not consume much electrical energy. However, they mainly rely on cylinders to drive magnet blocks to control the operation of the PMER. The control structure is more complex, and the constant magnetic characteristics of permanent magnet materials increase the difficulty of control [4–6]. Therefore, adopting a hybrid excitation method of the permanent magnet and the electromagnetic will be a more reasonable choice for ECRs.

To overcome the shortcomings of traditional ECRs in braking performance, many scholars have developed new types of ECRs. Li developed a series of eddy current hydraulic composite retarders to compensate for the insufficient braking power of ECRs at high speeds [7–10]. Zhao developed a permanent magnet eddy current heater based on a Halbach array, which has higher heat generation efficiency compared to traditional eddy current heaters [11]. Gulec proposed a hybrid excitation ECR that adopts a parallel magnetic circuit structure with electromagnetic excitation as the main and permanent magnet excitation as the auxiliary. It has the advantages of easy control, a large air-gap magnetic flux density, and high braking power density but does not consider the problem of eddy current thermal degradation [12].

In this paper, based on the introduction of the structure and working principle of the hybrid excitation rotary electromagnetic retarder (HERER), theoretical analysis and finite element simulation analysis were conducted on the HERER, and, finally, the braking performance of the HERER was tested on a bench.

2. Structure and Working Principles

The structure of the proposed HERER is shown in Figure 1a, which mainly consists of a stator, a rotary drum, and an electronic control unit. The stator part includes excitation coils, stator iron cores, and permanent magnets. The permanent magnets are fixed between the stator magnetic shoes, and the magnetic directions between adjacent permanent magnets are opposite. The magnetic field generated by the excitation coils fixed on the stator pole when a direct current is applied in the same direction as the magnetic field generated by the permanent magnets, forming a parallel magnetic circuit structure, thereby improving the air-gap magnetic flux density of the HERER. When a direct current is applied to the HERER, the rotating drum that rotates with the drive shaft will cut the magnetic field lines emitted by the stator and generate eddy currents. The induced magnetic field formed by the eddy currents interacts with the original excitation magnetic field to generate braking torque. During this process, Joule heat is generated on the surface of the drum, which is carried away by the air flowing around the HERER. Pulse width modulation (PWM) is applied to the current provided by the vehicle battery, enabling torque control of the HERER.
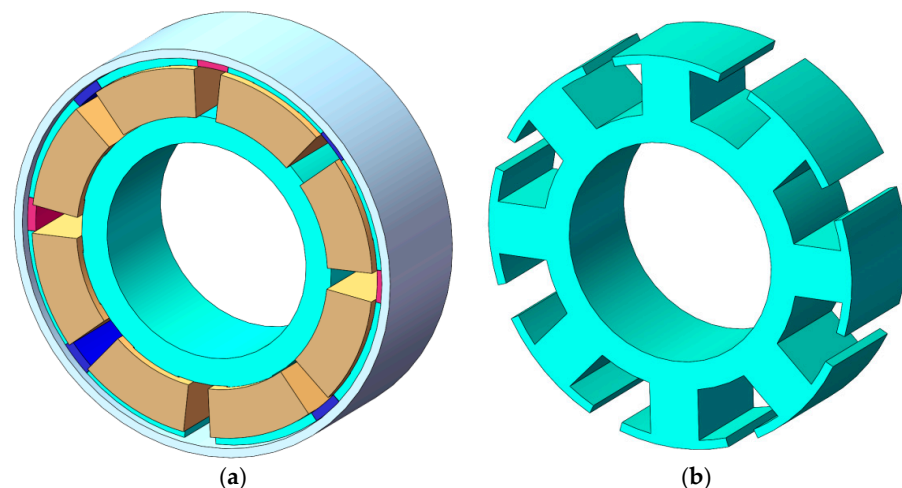

Figure 1. (**a**) Overall structure of the HERER. (**b**) The rotor of the HERER.

When the HERER is not working, the electronic control unit does not energize the excitation coil, and the magnetic field formed by the circumferential magnetized permanent magnet is closed through the stator. The magnetic field does not pass through the rotor, and the magnetic field distribution is shown in Figure 2a. At this time, the HERER will not generate braking torque. When the HERER is working, the electronic control unit supplies power to the excitation coil, and the magnetic field generated by the coil forces the magnetic field generated by the permanent magnets to pass through the rotor together. The magnetic field distribution is shown in Figure 2b. At this time, the rotor cuts the magnetic field lines emitted by the stator, thereby generating braking torque. The HERER uses air cooling to cool the surface of the rotating drum that generates eddy currents. In terms of the excitation method, the HERER adopts a hybrid excitation of the permanent magnet and electromagnetic to enhance the air-gap magnetic flux density, thereby improving the braking power density and saving electrical energy.
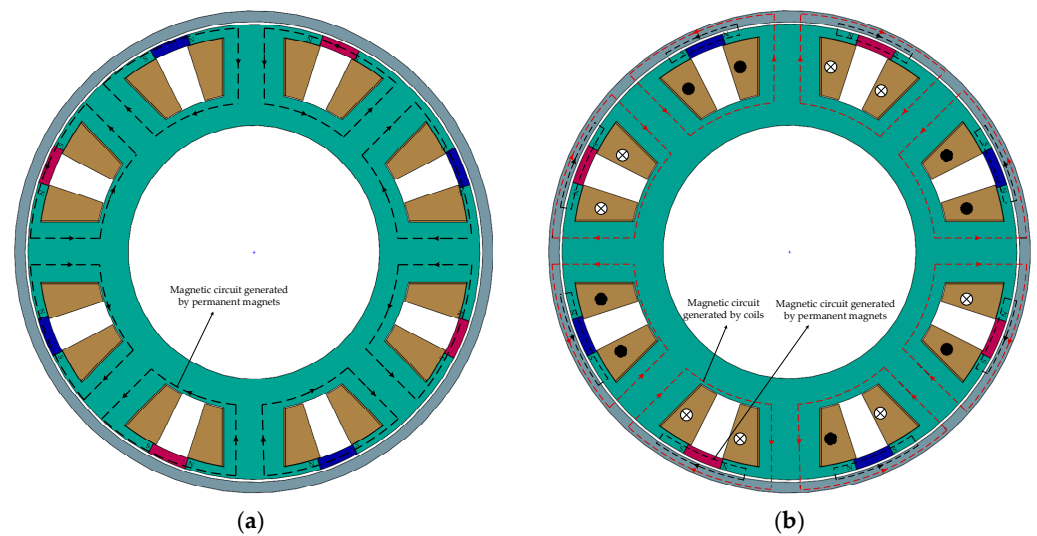
Figure 2. (**a**) Internal magnetic circuit of the HERER when not braking. (**b**) Internal magnetic circuit of the HERER when braking.

3. Equivalent Magnetic Circuit Model

Considering the symmetry of the structure of the HERER, the established analysis model is 1/4 of the actual structure, as shown in Figure 3. According to Figure 3, an equivalent magnetic circuit analysis model is established, as shown in Figure 4.
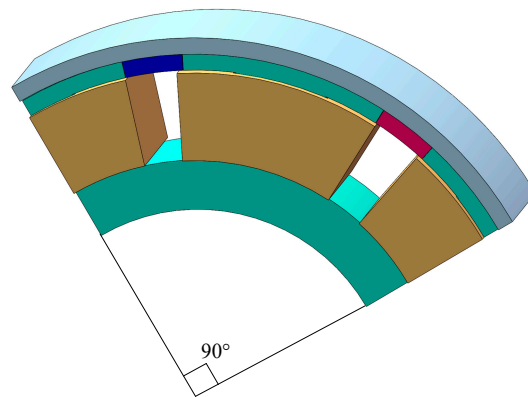

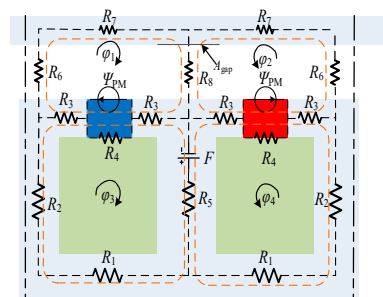Figure 3. Theoretical analysis model.

Figure 4. Equivalent magnetic circuit analysis model during braking.

The relationship between the magnetic flux, magnetic resistance, and magnetic potential of each branch in the equivalent magnetic circuit satisfies Kirchhoff's law and can be expressed by the following equation:

$$
\begin{bmatrix} \varphi_1 \\ \varphi_2 \\ \varphi_3 \\ \varphi_4 \end{bmatrix} = \begin{bmatrix} Z_{m1} & R_8 & Z_{m2} & 0 \\ R_8 & Z_{m1} & 0 & Z_{m2} \\ Z_{m2} & 0 & Z_{m3} & R_5 \\ 0 & Z_{m2} & R_5 & Z_{m3} \end{bmatrix}^{-1} \begin{bmatrix} \psi_{pm}R_4 \\ \psi_{pm}R_4 \\ F - \psi_{pm}R_4 \\ F - \psi_{pm}R_4 \end{bmatrix} \tag{1}
$$

$$
Z_{m1} = 2R_3 + R_4 + R_6 + R_7 + R_8 \tag{2}
$$

$$
Z_{m2} = -2R_3 + R_4 \tag{3}
$$

$$
Z_{m3} = R_1 + R_2 + 2R_3 + R_4 + R_5 \tag{4}
$$

$$
F = NI \tag{5}
$$

$$
\psi_{pm} = \frac{H_c h_m}{R_4} \tag{6}
$$

where N is the number of turns of the coil, I is the current of the coils, H_c is the coercivity of the permanent magnet, and h_m is the thickness of the permanent magnet.

$R_1 \sim R_8$ in the formula can be calculated by the following equation:

$$
R_i = \frac{l_i}{\mu_i S_i}, \ i = 1 \sim 8 \tag{7}
$$

where l_i is the length of the magnetic flux passing through, S_i is the equivalent cross-sectional area of the magnetic flux passing through, and μ_i is the magnetic permeability, which can be calculated using the iterative method proposed in the previous literature [13].

The static air-gap flux density is a function of angle θ, which satisfies the following equation:

$$
B_0(\theta) = \frac{\varphi_{gap}}{A_{gap}} \tag{8}
$$

where A_{gap} is the cross-sectional area through which the air-gap magnetic field flows and φ_{gap} is the air-gap magnetic flux.

When the HERER brakes, the rotating drum induces eddy currents within a certain depth on its inner surface. The induced magnetic force generated by the eddy currents has a significant impact on the size and distribution of the original static air-gap magnetic flux density. Therefore, the transient resultant air-gap magnetic flux density satisfies the following equation:

$$
B_\delta(\theta) = B_0(\theta) + B_i(\theta) \tag{9}
$$

where $B_i(\theta)$ represents the air-gap magnetic density generated by eddy currents.

The eddy current density generated within a certain depth of the rotor during the braking process can be calculated as follows:

$$
J = \sigma[r_r \omega \times B_\delta(\theta)]e^{-d/\delta} \tag{10}
$$

where σ is the conductivity of the rotor, r_r is the effective working radius of the rotor, ω is the angular velocity of the rotor, d is the thickness of the rotor, and δ is the skin depth. The skin depth satisfies the following equation:

$$
\delta = \sqrt{\frac{2}{\omega \mu \sigma}} \tag{11}
$$

The HERER converts the kinetic energy of a vehicle into thermal energy, and the braking power and braking torque satisfy the following equations:

$$
p_e = \iiint \frac{J^2}{\sigma} dV \tag{12}
$$

$$T = \frac{p_{\mathrm{e}}}{\omega} \tag{13}$$

where V is the volume within the skin depth δ.

4. Finite Element Analysis

To predict the electromagnetic characteristics, such as the air-gap flux density and eddy current torque of the HERER, a finite element analysis is conducted on the HERER. The finite element analysis software used is the electromagnetic field analysis software Jmag-Designer 14, developed by the Japan Institute of Integrated Research. The size design and rotor performance parameters of the HERER model are shown in Table 1.

Table 1. Dimensional design and rotor performance parameters of the HERER.

Size Parameters of Retarder	Value	Parameters of Rotor Material	Value
Axial length of retarder L [mm]	65	Conductivity σ [S/m]	4×10^6
Stator radius r_{s} [mm]	200	Heat capacity C_{s} [J/kg·K]	460
Rotor Radius r_{r} [mm]	200	Thermal conductivity λ [W/m·K]	44
Rotor thickness d [mm]	9.2	Density ρ [kg/m^3]	7870
Thickness of permanent magnet h_{m} [mm]	13.5		

During simulation, it is assumed that the electromagnetic properties of the material are not affected by temperature, and the HERER does not leak magnetic flux to its attached automotive components. The materials for the stator and rotor of the HERER are selected as No. 10 steel, the coil material is selected as copper, and the permanent magnet material is selected as Nd-Fe-B (N38SH); the conductivity of the rotor is set to 4×10^6 S/m. The mesh size of each part of the HERER is set to 10 mm. Considering the dynamic variation of the air-gap magnetic field, the stator magnetic poles and the rotor surface are set to 3 mm. The mesh distribution of the simulation model is shown in Figure 5. The elements of the simulation model are 103,884, and the nodes are 39,968.
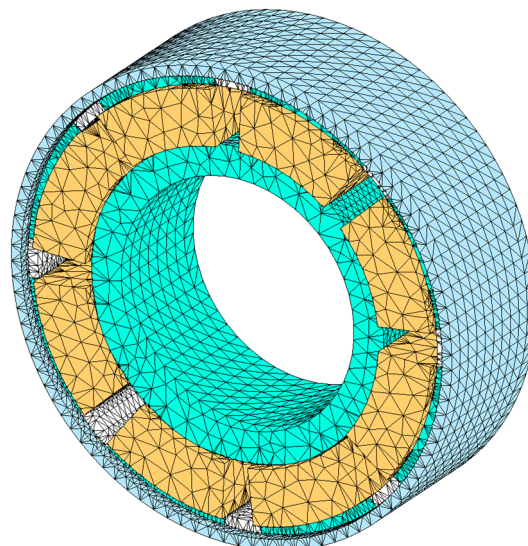

Figure 5. Three-dimensional finite element simulation model of the HERER.

4.1. Static Electromagnetic Field Simulation

To study the magnetic field distribution when the HERER is not braking, the current of the excitation coils is set to 0 A during simulation, and the obtained magnetic field contour plots and magnetic field vector plots are shown in Figures 6 and 7. From the Figures,

it can be seen that, when the HERER is not working, the magnetic field formed by the circumferential magnetized permanent magnets is closed by the stator, and the magnetic field does not pass through the rotor. The magnetic field is mainly concentrated on the magnetic shoes of the stator, with a maximum magnetic field density of 1.35 T.
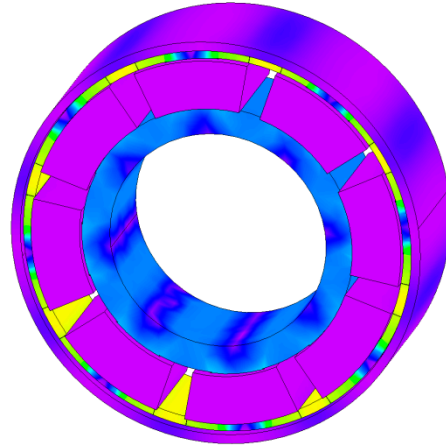

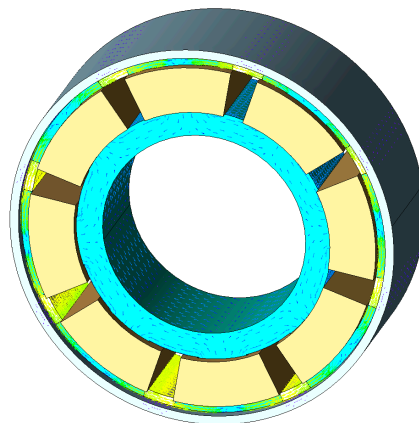**Figure 6.** Static magnetic field contour plots of the HERER.

Figure 7. Static magnetic field vector plots of the HERER.

To study the magnetic field distribution during the operation of the HERER, the current of the excitation coils is set to 40 A during simulation, and the obtained magnetic field contour plots and magnetic field vector plots are shown in Figures 8 and 9. From Figure 9, it can be seen that, when the HERER is working, the magnetic field generated by the coil forces the magnetic field generated by the permanent magnets to pass through the drum together. The magnetic field is mainly concentrated on the drum, with a maximum magnetic field density of 2.0 T.

Static air-gap magnetic flux density is an important reference indicator for the design of ECRs, which can reflect the saturation degree of the magnetic field inside ECRs and preliminarily predict the eddy current braking ability. Therefore, simulations are conducted with excitation currents set at 5, 10, 20, 30, and 50 A, and the static air-gap flux densities obtained at different currents are shown in Figure 10. From Figure 10, it can be seen that, as the excitation current increases, the air-gap flux density first increases rapidly and then increases slowly. When the excitation current is 5 A, the amplitude of the air-gap flux density is 0.32 T. When the excitation current continues to increase and exceeds 30 A, the air-gap flux density is significantly higher at $\pm(0.3{\sim}0.5)$ compared to other regions. When the excitation circuit is 40 A, the amplitude of the air-gap flux density is around 0.73 T.
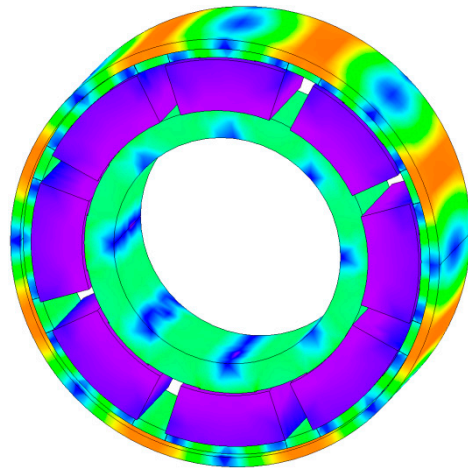
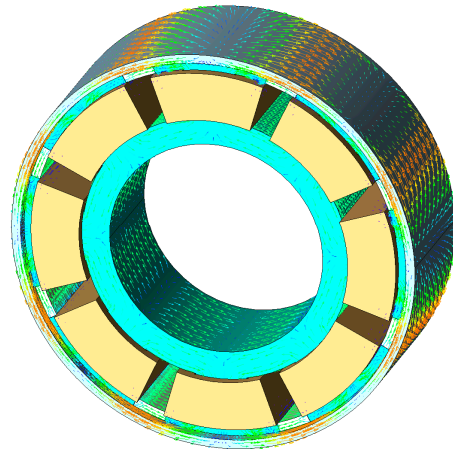**Figure 8.** Transient magnetic field contour plots of the HERER.

Figure 9. Transient magnetic field vector plots of the HERER.
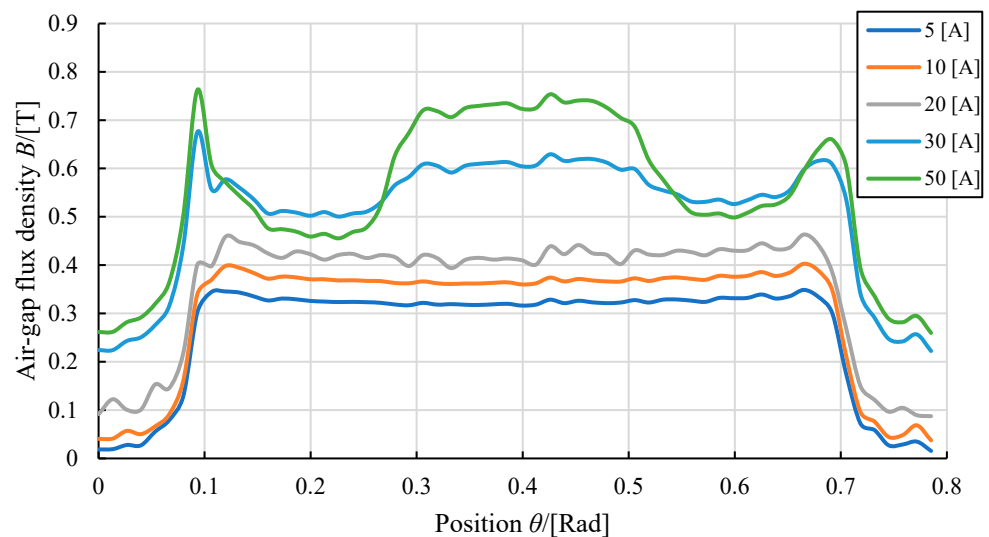

Figure 10. Static air-gap flux density of the HERER under different currents.

To compare the electromagnetic characteristics of a pure electric excitation retarder, a simulation model of the pure electric excitation retarder is established based on the structural design parameters of the HERER, as shown in Figure 11. The established pure electric excitation retarder model has the same design parameters as the HERER, except that eight pairs of permanent magnets are missing. Simulate the excitation currents of

the two types of retarders with 10 A and 50 A, respectively, and obtain the static air-gap flux density, as shown in Figure 12. From Figure 12, it can be seen that, under the same excitation current, the air-gap flux density of the hybrid excitation retarder is higher than that of pure electric excitation. When the current is 10 A, the amplitude of the air-gap flux density of the pure electric excitation retarder is 0.37 T. When the current increases to 50 A, the overall air-gap flux density increases, especially at 0.3–0.5, where the amplitude of the air-gap flux density is 0.83 T. However, the air-gap flux density significantly decreased at 0.1–0.25 and 0.54–0.65. When the current is 10 A, the amplitude of the air-gap flux density of the HERER is 0.42 T. When the current increases to 50 A, the air-gap flux density increases overall, especially slightly at 0.3–0.5, and there is no significant decrease in the air-gap flux density in other areas.
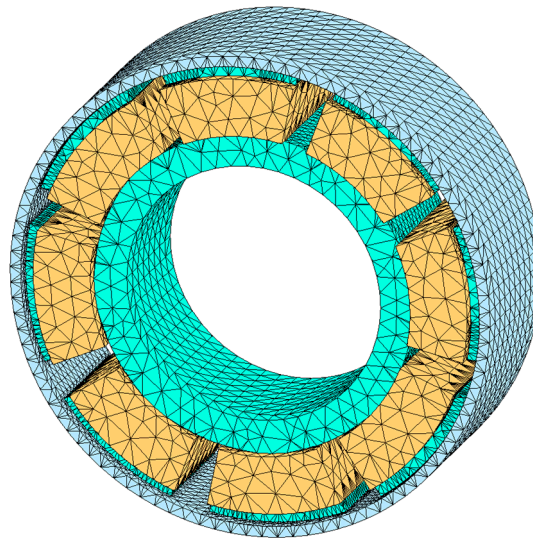

Figure 11. Finite element simulation model of the pure electric excitation retarder.
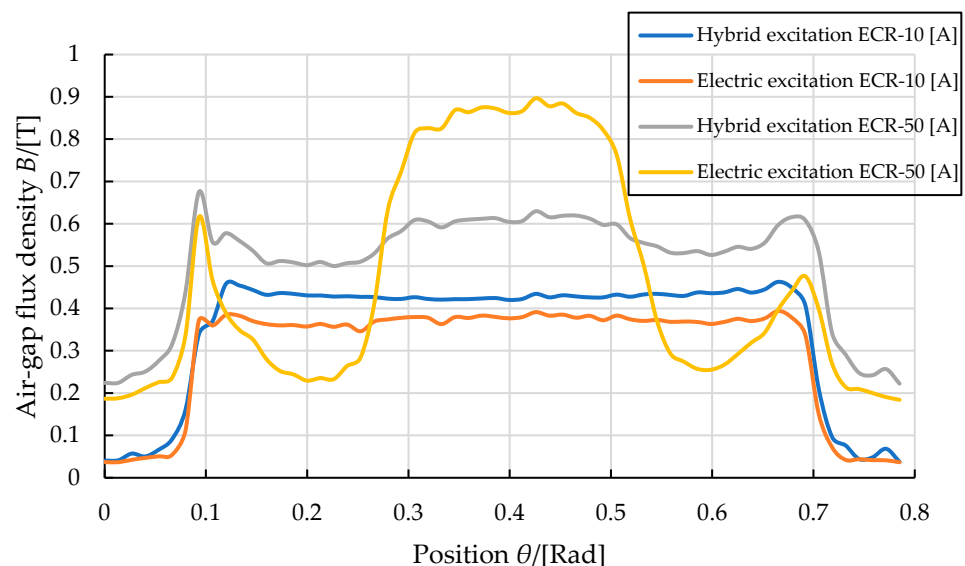

Figure 12. Comparison of the static air-gap flux density between the HERER and the pure electric excitation retarder.

4.2. Transient Electromagnetic Field Analysis

To obtain the transient air-gap flux density at different speeds, the excitation currents of the HERER and the pure electric excitation retarder are set to 50 A, and the speeds are

set to 0, 500, 1000, 1500, and 2000 r/min, respectively. The simulation results are shown in Figures 13 and 14.
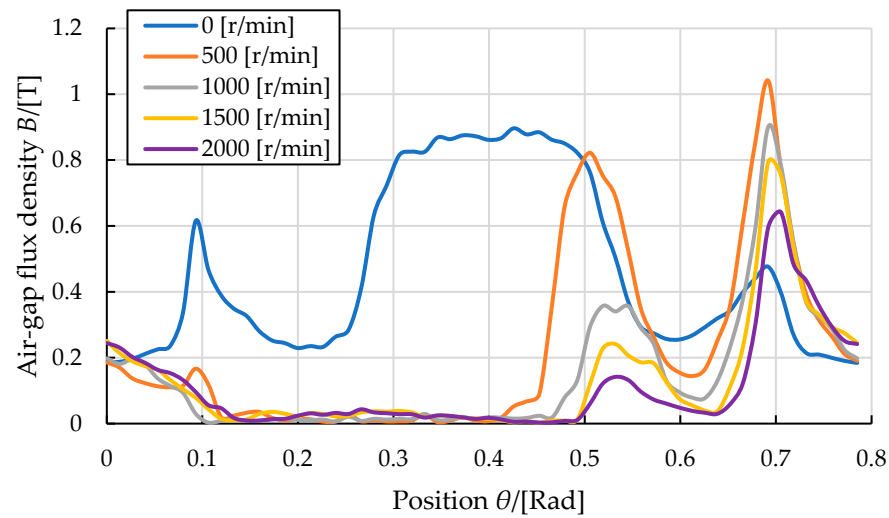

Figure 13. Transient air-gap flux density of the pure electric excitation retarder at different speeds.
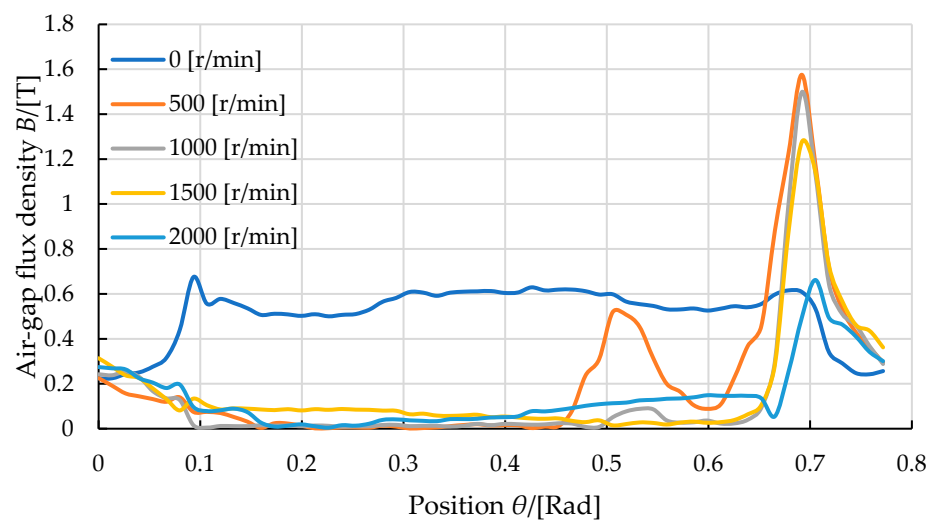

Figure 14. Transient air-gap flux density of the HERER at different speeds.

From Figures 13 and 14, it can be seen that, overall, the air-gap flux density of the HERER is higher than that of the pure electric excitation retarder. The air-gap flux density of both types of retarders decreases on one side and increases on the other side at different speeds. This phenomenon is caused by the eddy current effect and magnetic saturation of the ferromagnetic materials [14]. During one cycle, the eddy current has one side opposite the direction of the static air-gap magnetic field and the other side in the same direction as the static air-gap magnetic field. Due to the influence of magnetic saturation of ferromagnetic materials, the transient air-gap flux density decreases more than it increases.

As the rotational speed increases, the eddy current magnetomotive force gradually increases, and the weakening of the air-gap flux density becomes more pronounced. However, as the rotational speed increases, the reduction rate of transient air-gap flux density decreases. When the rotational speed is high enough, the air-gap flux density eventually tends to stabilize.

4.3. Eddy Current Braking Torque

To obtain the eddy current braking performance of the HERER and pure electric excitation retarder, the excitation currents are set to 20 and 40 A, respectively, and the rotor

speed is set from 0 to 2000 r/min. The simulation results are shown in Figure 15. From Figure 15, it can be seen that the HERER and the pure electric excitation retarder increase with the increase in the currents. The braking torque of both the HERER and the pure electric excitation retarder first increases and then gradually decreases with the increase in speed. However, the braking torque of the HERER is generally larger than that of the pure electric excitation retarder. When the excitation current is 50 A, and the speed is 1000 r/min, the braking torque of the HERER is 1560 Nm, while that of the pure electric excitation retarder is 1110 Nm.
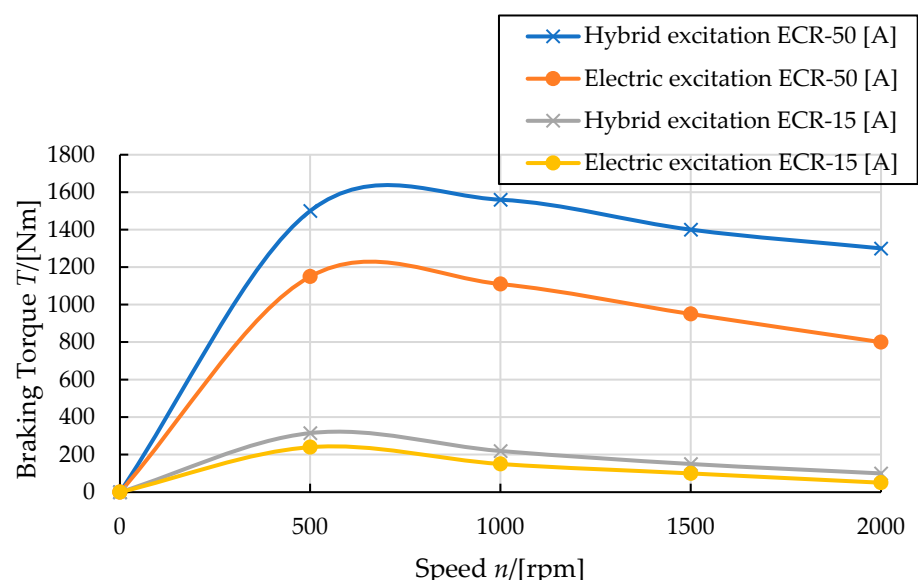

Figure 15. Braking torque of the HERER and the pure electric excitation retarder under different operating conditions.

5. Bench Test

The HERER test bench mainly consists of a prototype of the HERER, a high-power drive motor, a transmission device, a torque sensor, an adjustable excitation power supply, and a data acquisition system, as shown in Figure 16. Obtain the speed characteristic curve of the braking torque of the HERER through the retarder braking torque test. At the same time, compare the experimental data with the theoretical calculation values to verify the correctness of the theoretical calculations.

Figure 16. Test bench for HERER.

5.1. Residual Torque

Residual torque refers to the additional braking torque that the residual magnetism of air and permanent magnets bring to the vehicle transmission system when the HERER is in a non-braking condition. Residual torque can affect the starting performance of vehicles, increase fuel consumption, and is an important indicator of eddy current retarders.

Figure 17 shows the variation of residual torque with speed for the prototype of the HERER. From Figure 17, it can be seen that, as the rotational speed increases, the residual torque shows a trend of first increasing, reaching a peak, and then decreasing. When the speed is around 1000 r/min, the residual torque of the HERER is at its maximum, which is 0.88 Nm.
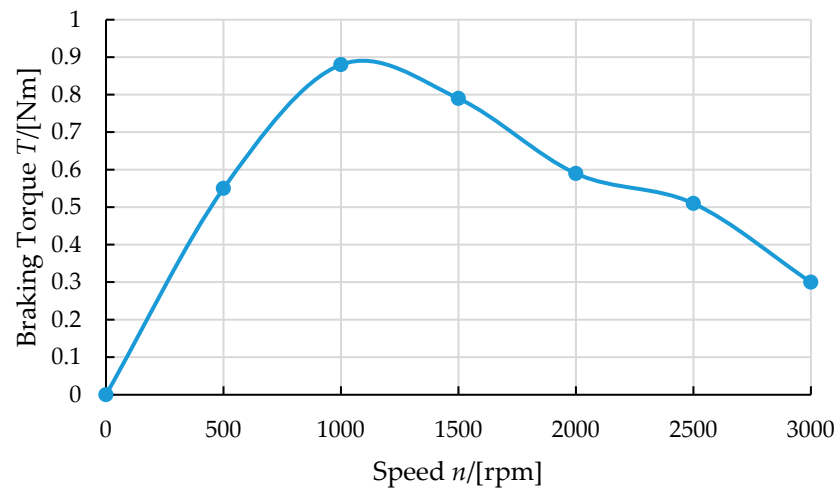

Figure 17. The law of residual torque of the HERER prototype changes with speed.

5.2. Eddy Current Braking Characteristics

To test the eddy current braking torque of the HERER at different currents, the excitation currents are set to 15 and 50 A, and the rotational speeds are set to 500, 1000, 1500, and 2000 r/min. The test results are shown in Figure 18. From Figure 18, it can be seen that the braking torque increases with the increase in excitation current. The braking torque at different currents first increases with speed, then reaches its peak, and, as the speed further increases, the braking torque will decrease with the increase in speed. When the speed is 1000 r/min and the speed is 50 A, the braking torque of the HERER is 1390 Nm.
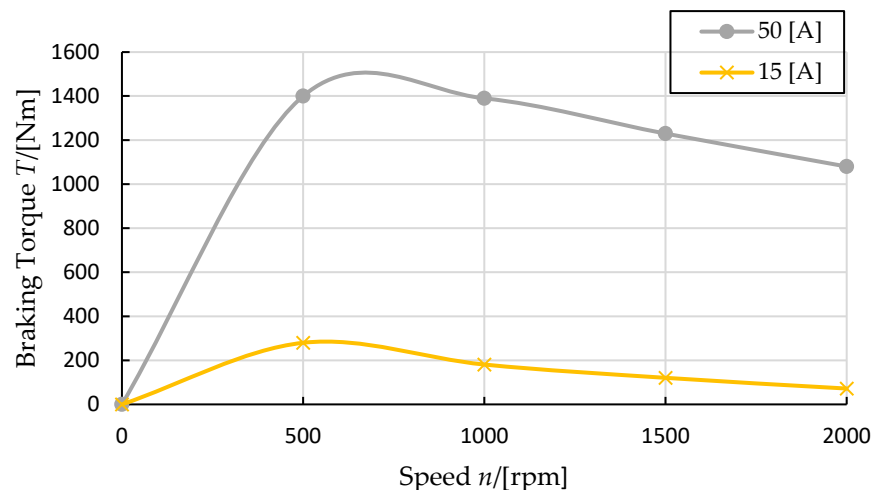

Figure 18. Test braking torque of the HERER under different operating conditions.

5.3. Theoretical Verification

As shown in Figure 19, when the excitation current is 50 A, and the speed is below 500 r/min, the FEM and the theoretical calculation values are in good agreement with the experimental values. When the speed exceeds 750 r/min, the error between the FEM and the theoretical calculation begins to increase, and, as the speed further increases, the error between the theoretical calculation values exceeds that of the FEM. The average relative

error of the FEM is 11.7%, with a maximum relative error of 17%, while the theoretically calculated average relative error is 17.7%, with a maximum relative error of 32%.
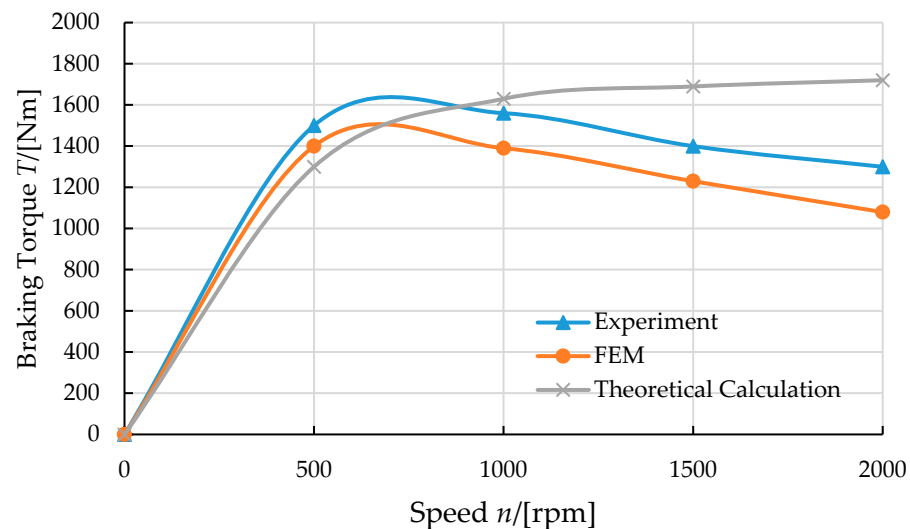

Figure 19. Comparison of theoretical calculation, FEM, and experimental braking torque curves.

When the rotational speed reaches a certain level and further increases, due to the skin effect, the electromagnetic field distribution in the HERER becomes significantly nonlinear, leading to an increase in the edge effect of its electromagnetic field. On the other hand, as the rotational speed increases, the eddy current thermal effect on the HERER rotor intensifies, and the increase in temperature leads to a decrease in the electrical conductivity and magnetic permeability of the material. Therefore, both of the above effects limit the increase in braking torque of the HERER at high speeds. However, the theoretical model proposed in this paper ignores the influence of these two effects. Therefore, when the speed is above 500–700 rpm, the calculation accuracy of the theoretical model will significantly decrease with the increase in speed. However, the finite element model did not consider the influence of eddy current thermal effects, resulting in higher calculation results than experimental tests.

6. Conclusions

A new type of HERER is proposed, and the equivalent magnetic circuit analysis model and finite element analysis model of the retarder are established. The finite element method was used to analyze the magnetic field distribution, air-gap flux density, and braking torque inside the retarder under different operating conditions. The effectiveness of the finite element analysis model and equivalent magnetic circuit analysis model was verified through bench tests.

References

1. Anwar, S. A parametric model of an eddy current electric machine for automotive braking application. *IEEE Trans. Control Syst. Technol.* **2004**, *12*, 422–427. [CrossRef]
2. Jiao, B.; Li, D.; Du, X.; Zhang, K. Performance analysis and experimentation of a liquid-cooled eddy current retarder with a dual salient poles design. *IEEE Trans. Energy Convers.* **2014**, *29*, 84–90. [CrossRef]
3. Zhang, K.; Li, D.; Zheng, R.; Yin, W. Design and performance of a self-excited and liquid-cooled electromagnetic retarder. *IEEE Trans. Veh. Technol.* **2015**, *64*, 13–20. [CrossRef]
4. Ye, L.; Li, D.; Ma, Y.; Jiao, B. Design and Performance of a Water-cooled Permanent Magnet Retarder for Heavy Vehicles. *IEEE Trans. Veh. Technol.* **2011**, *26*, 953–958. [CrossRef]
5. Kou, B.; Jin, Y.; Zhang, H.; Zhang, L.; Zhang, H. Nonlinear analytical modeling of hybrid-rxcitation double-sided linear eddy-current brake. *IEEE Trans. Magn.* **2015**, *11*, 8003404.
6. Kou, B.; Jin, Y.; Zhang, H.; Zhang, L.; Zhang, H. Modeling and analysis of force characteristics for hybrid excitation linear eddy current brake. *IEEE Trans. Magn.* **2014**, *50*, 8001205. [CrossRef]
7. Tian, J.; Li, D.; Ye, L. Study on braking characteristics of a novel eddy current-hydraulic hybrid retarder for heavy-duty vehicles. *IEEE Trans. Energy Convers.* **2020**, *35*, 1658–1666. [CrossRef]
8. Gao, Z.; Li, D.; Tian, J.; Ning, K.; Ye, L. Design and performance analysis of a novel radially distributed electromagnetic-hydraulic retarder for heavy vehicles. *IEEE Trans. Energy Convers.* **2022**, *37*, 892–900. [CrossRef]
9. Zhang, K.; Shang, H.; Xu, J.; Niu, J.; Yue, Y. Testing and performance analysis of an integrated electromagnetic and hydraulic retarder for heavy-duty vehicles. *Eng. Appl. Artif. Intel.* **2023**, *126*, 106906. [CrossRef]
10. Tian, J.; Li, D.; Ning, K.; Ye, L. Research on heat dissipation optimization of a novel liquid-cooling eddy current brake. *IEEE Trans. Energy Convers.* **2021**, *36*, 131–138. [CrossRef]
11. Zhao, L.; Peng, Y.; Sha, C.; Li, R.; Xu, Y. Permanent magnet type eddy current heater based on cylindrical halbach array for reducing oil's viscosity. *IEEE Trans. Appl. Supercond.* **2010**, *20*, 865–869. [CrossRef]
12. Gulec, M.; Aydin, M.; Nerg, J.; Lindh, P.; Pyrhonen, J. Magneto-thermal analysis of an axial-flux permanent-magnet-assisted eddy-current brake at high-temperature working conditions. *IEEE Trans. Ind. Electron.* **2021**, *68*, 5112–5121. [CrossRef]
13. Mohammadi, S.; Mirsalim, M.; Vaez-Zadeh, S. Nonlinear modeling of eddy-current couplers. *IEEE Trans. Energy Convers.* **2014**, *29*, 224–231. [CrossRef]
14. Corti, F.; Grasso, F.; Paolucci, L.; Pugi, L.; Luchetti, L. Circular coil for EV wireless charging design and optimization considering ferrite saturation. In Proceedings of the 5th International Forum on Research and Technologies for Society and Industry: Innovation to Shape the Future, Florence, Italy, 9–12 September 2019.